Torque Resistance Analysis and Dynamic Trajectory Planning for 3-DOF Cable Suspended Parallel Robot With Parallelogram Cable Loops

Hanqing Liu, Jinhao Duan, Zhufeng Shao, Stéphane Caro

Torque Resistance Analysis and Dynamic Trajectory Planning for 3-DOF Cable Suspended Parallel Robot with Parallelogram Cable Loops

Hanqing Liu[1], Jinhao Duan[1], Zhufeng Shao*[,1], Stéphane Caro[2], *Member, IEEE*,

***Abstract*—This letter investigates the torque resistance performance and dynamic trajectory planning methods for general 3-DOF Cable Suspended Parallel Robots (CSPRs) with parallelogram cable loops, aiming to offer efficient and lightweight robotic equipment for industrial applications. The Torque Resistance Ability Index (TRAI) and Torque Resistance Consumption Index (TRCI) are proposed to evaluate the torque resistance performance of parallelogram cable loops and CSPRs. The Fourier model is adopted to plan the dynamic trajectory of the CSPR with the proposed TRAI and TRCI, which effectively minimizes oscillations and avoids overturns of the moving platform. The B-spline model is employed to implement more complex dynamic trajectories that go through additional constraint points, enhancing flexibility and adaptability. A prototype of the CSPR with parallelogram cable loops is established, and the proposed indexes and trajectory planning methods are verified with experiments.**

***Index Terms*——Cable-suspended parallel robot (CSPR), torque resistance, dynamic trajectory, parallelogram cable loop**

I. Introduction

Cable-suspended parallel robots (CSPRs) are a class of cable-driven parallel robots (CDPRs) that rely on gravity to keep the cable tensioned [1]. CSPRs have outstanding performance in large workspaces [2], [3], [4], and heavy loads [5] which have been adopted in photography [6], logistics [7], [8], construction [9], [10] and etc.

In most industrial logistics, translational motion with good rotational stability is required for robots. Parallelogram cable loops have been introduced to CSPRs to eradicate the tilting of the end-effector and therefore have greatly enhanced the ease of deployment and use of CSPRs [11], [12]. Parallelogram cable loops were first proposed in [13], and already adopted in CDPRs for 3D printing [14], construction [9], [10] and transportation [15].

A. Dynamic Trajectory Planning

To expand the motion range of CSPRs beyond the static workspace, Gosselin first proposed the point-to-point dynamic trajectory for two-DOF CSPRs considering the terminal acceleration and inertial force [16], [17], and extended the method to three-DOF CSPRs [18], [19]. Jiang designed dynamic trajectories for a three-DOF planar CSPR in [20], considering the rotational DOF, and proposed the basis motion for point-to-point dynamic trajectories of six-DOF Stewart CSPRs [21].

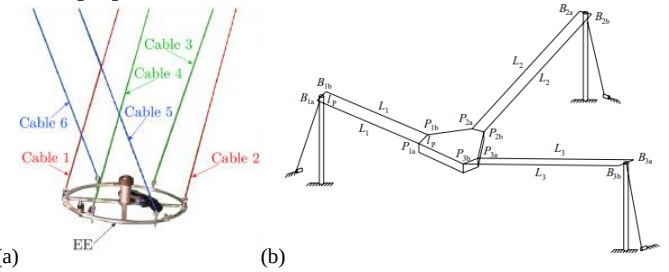

Fig. 1. Special configuration (a) and general configuration (b) of CSPR with parallelogram cable loops [13], [23].

Extensive research has been conducted on the dynamic trajectory planning of CSPRs driven by individual cables. However, the exploration of CSPR with parallelogram cable loops is still in its infancy, with limited studies addressing its dynamic trajectory planning. Longval analyzed the rotational sensitivity of planer CSPRs with diverse configurations. His research demonstrated that the parallelogram structure outperforms the non-parallelogram structure in terms of rotational stability and achieving purely translational trajectories. Additionally, he highlighted that an effective way to maximize the size of the static and dynamic workspace was to employ an end-effector which could be dynamically equivalent to a point mass end-effector [22]. This special configuration (architecture) was proposed and thoroughly analyzed in [23], as shown in Fig. 1(a). Lines connecting the end-effector connection points of each set of parallelogram cable loop intersect at one point P, and the resultant wrench has zero moment about the point P. Specifically, when only gravity and inertia forces are taken into account, point P coincides with the center of mass. While the special configuration offers advantages such as torque balance and simplified dynamic trajectory implementation through equivalence to a point-mass

Manuscript received: January 3, 2024; Revised April 10, 2024; Accepted May 6, 2024.

This paper was recommended for publication by Editor Pallottino, Lucia upon evaluation of the Associate Editor and Reviewers' comments. This work was supported by the National Key R&D Program of China (No. 2022YFC3601100).

[1]Hanqing Liu, Jinhao Duan and Zhufeng Shao are with:

[a]State Key Laboratory of Tribology & Institute of Manufacturing Engineering, Department of Mechanical Engineering, Tsinghua University, Beijing 100084, China (E-mail: shaozf@mail.tsinghua.edu.cn).

[b]Beijing Key Lab of Precision/Ultra-precision Manufacturing Equipment and Control, Department of Mechanical Engineering, Tsinghua University, Beijing 100084, China (E-mail: shaozf@mail.tsinghua.edu.cn).

[2]Stéphane Caro is with CNRS at LS2N, Nantes Université, CNRS, Nantes, France (E-mail: Stephane.Caro@ls2n.fr).

Digital Object Identifier (DOI): see top of this page.

configuration, it poses demanding requirements that are challenging to achieve in practice. Conversely, the general configuration depicted in Fig. 1(b) is more practical and versatile [13]. However, ensuring torque balance emerges as a critical concern for the general configuration, leading to complex torque analysis, diminished static workspaces, and challenges in dynamic trajectory planning. The central challenge lies in determining the force distribution within the parallelogram cable loop under the resultant wrench. This letter emphasizes the torque resistance analysis of general CSPRs with parallelogram cable loops, which inspires new indexes and an improved dynamic trajectory planning method.

Existing researches on dynamic trajectory planning primarily focuses on verifying the feasibility of dynamic trajectories with Fourier and polynomial models [17] and [19], [20], [21]. However, in practical applications where stability and flexibility are required, performance of dynamic trajectories needs to be considered. To address this issue, the Torque Resistance Ability Index (TRAI) and Torque Resistance Consumption Index (TRCI) are proposed to evaluate the torque resistance performance of parallelogram cable loops and CSPRs, and are adopted to improve dynamic trajectory planning method. In addition to commonly used Fourier model, the B-spline model known for its capability in handling complex trajectory planning [24] is introduce to the dynamic trajectory for the first time to add midpoint constraints and improve the flexibility. This letter transcends mere feasibility, aiming to elevate the performance of dynamic trajectories, with a specific focus on enhancing stability, flexibility and adaptability. It achieves this by proposing innovative torque indexes and planning methods.

B. Available Wrench Set and Resistance Ability

The available wrench set of CSPRs is defined as a set spanned by the available wrench of each cable in the wrench space [25]. The available wrench set indicates the force and torque output or resistance ability of CSPRs, which is a kernel consideration in the design and optimization stages to analyze the workspace [26], acceleration performance [27], and disturbance resistance ability [28], [29].

The available wrench set is straightforward for CSPR with few DOFs, such as planar or point-mass CSPR. For CSPR with finite-extension moving platform in space, the available wrench set becomes complex and challenging to visualize. In the case of CSPRs with parallelogram cable loops, which are the focus of this letter, the available wrench set constitutes a complex twelve-hyperplane body in six-dimensional space, comprising three force dimensions and three torque dimensions. To study the performance of CSPRs intuitively, Erskine evaluated the cross-section of the available wrench set under specific force or torque conditions [30]. The projection of the available wrench set on the hyperplane is adopted to improve computational efficiency [31] and to analyze the impact of specified directional auxiliary forces on the wrench set expansion [32].

However, the methods mentioned above may suffer from a significant loss of information. This letter capitalizes on the translational feature of CSPRs and the force distribution attribute within parallelogram cable loops. It introduces a groundbreaking method: the decoupled analysis of available force and torque sets. Consequently, it suggests novel indexes, namely the TRAI and TRCI, which focus on torque resistance characteristics rather than the force resistance performance of CSPRs [33], [34].

C. Contributions

In this letter, we conduct torque resistance analysis and dynamic trajectory planning for CSPRs with general configuration. The main contributions are as follows:

1) Decoupling of force and torque spaces: We achieve independent analysis of force and torque resistance performances for CSPRs with parallelogram cable loops.
2) Introduction of Torque Resistance Ability Index and Torque Resistance Consumption Index: These indexes are defined to illustrate the ability of the moving platform to resist torque disturbances effectively.
3) Proposal of an improved dynamic trajectory planning method: Leveraging the Fourier model and incorporating the established TRAI and TRCI, this method aims to reduce terminal oscillations in classical point-to-point motion. Experimental verification demonstrates its effectiveness.
4) Promotion of flexible dynamic trajectories for industrial applications: We introduce a novel dynamic trajectory planning method based on the B-spline model, enhancing adaptability and versatility in real-world scenarios.

II. Torsional Resistance Analysis

A. Kinematics and Dynamics

The three-DOF translational CSPR is illustrated in Fig. 1. The parallelogram cable loop is composed of parallel cables that share an actuator with synchronized retraction and release, keeping the moving platform horizontal without rotation.

A base frame {O} is located on the base, a local frame {P} is attached to the barycenter of the moving platform (end effector), and axes are shown in Fig. 2. The *j*th cable in the *i*th parallelogram cable loop is marked as $A_{ij}B_{ij}$, where A_{ij} is the cable attachment point on the moving platform, and B_{ij} is the cable exit point of the base through pulleys.

When the position of the moving platform is given, cable vectors can be obtained as

$$\boldsymbol{l}_{ij} = \overrightarrow{B_{ij}A_{ij}} = \overrightarrow{OB_{ij}} - \overrightarrow{PA_{ij}} - \overrightarrow{OP}\,. \tag{1.}$$

The unit direction vector can be written as

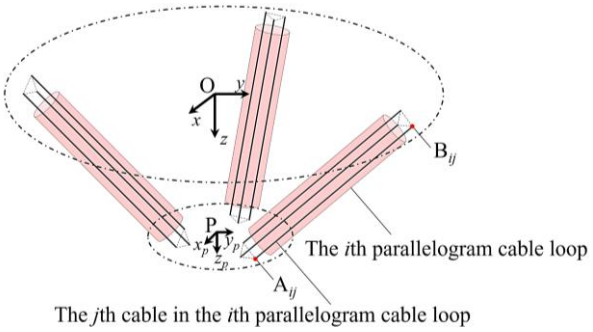

Fig. 2. Kinematic sketch of the three-DOF CSPR

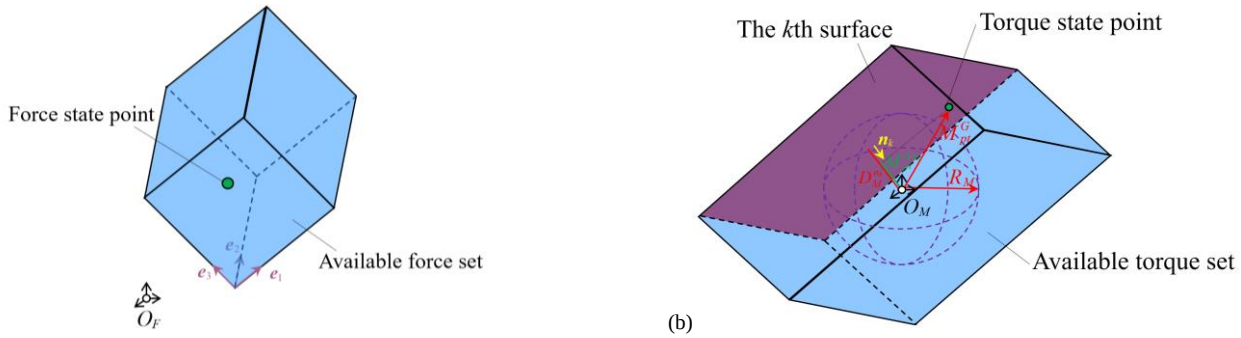

(a) (b)

Fig. 3. The available set and state point in (a) force space and (b) torque space.

$$\boldsymbol{e}_{ij} = \boldsymbol{l}_{ij} / \left|\boldsymbol{l}_{ij}\right| . \tag{2.}$$

Since the cables in the parallelogram cable loop are parallel, we can get

$$\boldsymbol{e}_{i1} = \boldsymbol{e}_{i2} = \cdots = \boldsymbol{e}_{in_i} = \boldsymbol{e}_i . \tag{3.}$$

where n_i is the number of cables in the ith parallelogram cable loop.

If only gravity and inertia forces are acting on the moving platform, the dynamic equilibrium of the CSPR is deduced as

$$\sum_{i,j} \boldsymbol{f}_{ij} + M\boldsymbol{g} = M\ddot{\boldsymbol{p}} \tag{4.}$$

$$\sum_{i,j} \boldsymbol{r}_{ij} \times \boldsymbol{f}_{ij} = 0 \tag{5.}$$

where $\boldsymbol{f}_{ij}$ is the cable tension of the jth cable in the ith parallelogram cable loop, M is the mass of the moving platform and load, $\boldsymbol{g}$ is the vector of gravitational acceleration, $\ddot{\boldsymbol{p}}$ is the acceleration vector of moving platform, $\boldsymbol{r}_{ij} = \overrightarrow{\mathrm{PA}_{ij}} - \overrightarrow{\mathrm{PC}}$, $i = 1,2,3\ j = 1,2,\ldots,n_i$, and the sum of gravity and inertial forces does not contribute to the moment equilibrium around the barycenter of moving platform.

To prevent cables from breaking or slacking, it is crucial to maintain cable tensions within the prescribed minimum and maximum values as

$$f_{\min} \le f_{ij} \le f_{\max},\ \ i = 1,2,3\ \ j = 1,2,\ldots,n_i . \tag{6.}$$

B. Decoupling of Force and Torque spaces

The cable tensions of a parallelogram cable loop can be determined as

$$F_i\boldsymbol{e}_i = \sum_j f_{ij}\boldsymbol{e}_i = \sum_j \boldsymbol{f}_{ij} \tag{7.}$$

where F_i is tension of the equivalent cable for the ith parallelogram cable loop.

Substituting (7) into (6), tension constraints for the equivalent cables can be obtained as

$$0 \le F_i / n_i \le f_{\max},\ \ i = 1,2,\ldots\ . \tag{8.}$$

Substituting (7) into (4), the force balance equilibrium can be written as

$$\sum_i F_i\boldsymbol{e}_i = M\left(\ddot{\boldsymbol{p}} - \boldsymbol{g}\right). \tag{9.}$$

Each inequality in (8) can be represented as a feasible line segment in force space corresponding to the respective cable direction. The force available set of the CSPR can be derived by computing the Minkowski sum of these feasible line segments. The force state point is located at $M\left(\ddot{\boldsymbol{p}} - \boldsymbol{g}\right)$ in force space. When the rotational DOFs of the moving platform are fully constrained by the parallelogram cable loops, the available force set and state point become decoupled from the six-dimensions available wrench set, as shown in Fig. 3(a), and can be analyzed independently and intuitively. When the number of drives is three, the equivalent tensions F_i can be determined based on the position of force state point.

To analyse the available torque set, the ith equivalent cable is determined on the moving platform with a virtual attachment point A_i, which satisfies

$$\overrightarrow{\mathrm{PA}_i} = \sum_j \lambda_{ij}\overrightarrow{\mathrm{PA}_{ij}} \tag{10.}$$

where $\sum_j \lambda_{ij} = 1, \lambda_{ij} > 0$.

Since the selection of A_i does not affect the torque equilibrium of the CSPR, in the following analysis, A_i is select on the point where $\lambda_{i1} = \lambda_{i2} = \ldots = \lambda_{in_i} = 1/n_i$.

The torque balance equilibrium (5) can be written as

$$\begin{aligned} \sum_{i,j} \boldsymbol{r}_{ij} \times \boldsymbol{f}_{ij} = 0 &\Leftrightarrow \sum_i \left(\sum_j \left(\boldsymbol{r}_i - \boldsymbol{r}_{ij}\right) \times \boldsymbol{f}_{ij} - \boldsymbol{r}_i \times \sum_j \boldsymbol{f}_{ij} \right) = 0 \\ &\Leftrightarrow \sum_{i,j} \boldsymbol{r}_i^{\,j} \times \boldsymbol{f}_{ij} = \sum_i \boldsymbol{r}_i \times \boldsymbol{F}_i \end{aligned} \tag{11.}$$

where $\boldsymbol{r}_i^{\,j} = \boldsymbol{r}_i - \boldsymbol{r}_{ij}$, $i = 1,2,\ldots\ j = 1,2,\ldots$ and $\boldsymbol{r}_i = \overrightarrow{\mathrm{PA}_i} - \overrightarrow{\mathrm{PC}}$, $i = 1,2,\ldots$.

The left side of the bottom equation in Eq. (11) is the torque supplied by the parallelogram cable loops, which is

$$\boldsymbol{M}_{tr} = \sum_{i,j} \boldsymbol{r}_i^{\,j} \times \boldsymbol{f}_{ij} . \tag{12.}$$

Considering the configurations consisting of equivalent cables instead of parallelogram cable loops, the moving platform could be tilt, and the parasitic tilting torque can be expressed as the right side of the bottom equation in Eq. (11)

$$\boldsymbol{M}_{pt} = \sum_i \boldsymbol{r}_i \times \boldsymbol{F}_i . \tag{13.}$$

Similar to the available set and state point in the force space, in the torque space, the set of all feasible $\boldsymbol{M}_{tr}$ is the available torque set, and $\boldsymbol{M}_{pt}$ is the torque state point as shown in Fig. 3(b). The available torque set and state point are determined by F_i solved in (9).

The available wrench set and the state point also represent the tension constraints: the state point moves with the external wrench, and the CSPR is feasible when the state point lies within the available set, considering both the force and torque.

C. Torque Resistance Indexes

To normalize the torque resistance performance indexes, the product of dimension and gravity of the moving platform is

defined as a reference torque, denoted as

$$M_g = mgr\,. \tag{14.}$$

where r is minimum enclosing circle radius of the cable attachment points.

In order to evaluate the torque-resistance ability of CSPR, Torque Resistance Ability Index (TRAI) was defined as

$$\text{TRAI} = M_g / R_M\,. \tag{15.}$$

where R_M is radius of the largest inscribed sphere.

The Geometry Center of the available torque set is located at [0, 0, 0], as shown in Fig. 4, and the parasitic-tilting torque $\boldsymbol{M}_{pt}$ describes the deviation of the state point from the Geometry Center. To indicate the torque-resistance consumption of the parasitic-tilting torque, Torque Resistance Consumption Index (TRCI) was defined as

$$\text{TRCI} = \max(M_{pt}^{n_1}/D_M^{n_1}, M_{pt}^{n_2}/D_M^{n_2}, ...)\,. \tag{16.}$$

where $D_M^{n_k}$ is the distance between the Geometry Center and the kth surface of available torque set, $M_{pt}^{n_k} = \boldsymbol{M}_{pt} \cdot \boldsymbol{n}_k$, and $\boldsymbol{n}_k$ is normal vector of the kth surface of available torque set.

The valid range of the TRAI and TRCI values is $[0, +\infty)$, and a necessary condition for CSPRs to be under control is TRCI≤1. The TRAI quantifies the size of the available torque set, which reflects the torque-resistance ability provided by the parallelogram cable loops. The TRCI represents the position of the state point in the torque space, indicating the proportion consumed to resist the parasitic-tilting torque. The combination of the TRAI and TRCI offers a comprehensive assessment of the CSPR's torque-resistance ability. Small values of both the TRAI and TRCI indicate excellent torque-resistance performance.

III. Dynamic Trajectory Planning

A. Improved dynamic trajectory with the Fourier model

The Fourier model is widely used for the point-to-point dynamic trajectory. Assume a series of prescribed zero-velocity target points $\mathbf{p}_i = [x_i, y_i]^T$ that need to be reached in sequence. The dynamic trajectory connected $\mathbf{p}_i$ and $\mathbf{p}_{i+1}$ are denoted as $\boldsymbol{H}_i(t)$. The dynamic trajectory based on the Fourier model can be expressed as

$$\boldsymbol{H}_i(t) = \begin{bmatrix} x_i(t) \\ y_i(t) \\ z_i(t) \end{bmatrix} = \begin{bmatrix} A_{xi} + B_{xi}\cos(\omega_i t) + C_{xi}\cos(2\omega_i t) \\ A_{yi} + B_{yi}\cos(\omega_i t) + C_{yi}\cos(2\omega_i t) \\ A_{zi} + B_{zi}\cos(\omega_i t) + C_{zi}\cos(3\omega_i t) \end{bmatrix} \tag{17.}$$

where the Fourier coefficients (for example, in the x-direction A_{xi}, B_{xi}, and C_{xi}) can be determined through position, velocity and acceleration constraints of target points in the ith trajectory segment, and ω_i is the frequency of the ith trajectory.

In previous works, the natural frequency of the equivalent pendulum at the height of the trajectory is adopted as the frequency of the ith trajectory, namely

$$\omega_i = \omega_{i,g} = \sqrt{2g/(z_i(t_i) + z_i(t_{i+1}))} \tag{18.}$$

where $\omega_{i,g}$ indicates the natural frequency.

In this letter, to enhance resistance to external torque and parasitic-tilting torque, an optimization goal for the dynamic trajectory is proposed as

$$\eta = avg(\text{TRAI})\big|_{W_T} \times avg(\text{TRCI})\big|_{W_T} \tag{19.}$$

where $avg(\text{g})\big|_{W_T}$ is the average value in the set of pose and motion state of the given dynamic trajectory.

The optimization goal η is employed to optimize the frequency ω_i of the dynamic trajectory, namely

$$\begin{aligned} &\min_{\omega_i} \quad \eta \\ &\textbf{\textit{s.t.}} \quad \omega_i \geq k\omega_{i,g} \end{aligned} \tag{20.}$$

where k is the constraint on the lowest frequency to ensure the efficiency. By utilizing the proposed indexes to formulate optimization goals, we aim to achieve comprehensive optimization of motion stability and efficiency.

B. Flexible Dynamic trajectory with the B-spline model

B-spline curves are employed to accommodate complex constraints of midpoints to cater to the diverse industrial requirements. The dynamic trajectory based on the k-order B-spline model is constructed as

$$\boldsymbol{H}_i(u) = \sum_{j=0}^{n_i} \boldsymbol{d}_{ij} N_{ij,k}(u) \tag{21.}$$

where $\boldsymbol{d}_{ij}$ is the jth control point, n is the number of control points, u is non-decreasing path parameter (time-dependent) and $N_{i,k}(u)$ is given by the De Boor formula

$$\begin{cases} N_{ij,0}(u) = \begin{cases} 1 & u_{ij} \leq u < u_{ij+1} \\ 0 & elsewhere \end{cases} \\ N_{ij,k}(u) = \dfrac{u - u_{ij}}{u_{ij+k} - u_i} N_{ij,k-1}(u) + \dfrac{u_{ij+k+1} - u}{u_{ij+k+1} - u_{i+1}} N_{ij+1,k-1}(u) \end{cases} \tag{22.}$$

where $[u_{i1}, u_{i2}, ..., u_{i(n+k+1)}]$ is a sequence of nodes. Control points and nodes can be determined through zero-velocity target points and non-zero-velocity midpoints.

As time t is a naturally non-decreasing parameter, u can be selected as t. The time t_i through target point is determined by the natural frequency

$$t_i = t_{i-1} + 2\pi/\omega_{i,g},\ t_0 = 0\,. \tag{23.}$$

Considering the stability and reliability of the dynamic trajectory, the comprehensive goal η is utilized to optimize the midpoint time $t_{i,mid}$.

$$\begin{aligned} &\min_{\omega_i} \quad \eta \\ &\textbf{\textit{s.t.}} \quad t_{i-1} < t_{i,mid} < t_i \end{aligned}\,. \tag{24.}$$

IV. Experimental Verification

A. Experiment Setup

The CSPR with parallelogram cable loops in the experiment is shown in Fig. 4(a). The mass of the moving platform is 5.3kg. Positions of cable attachment points and cable exit points are listed in Table I. The static workspace of this configuration is a regular hexagonal prism with a side length of 0.32m, as illustrated in Fig. 4(b). Its static workspace is only 56% of the CSPR in the special configuration in [23], making dynamic trajectory planning challenging and urgently necessary.

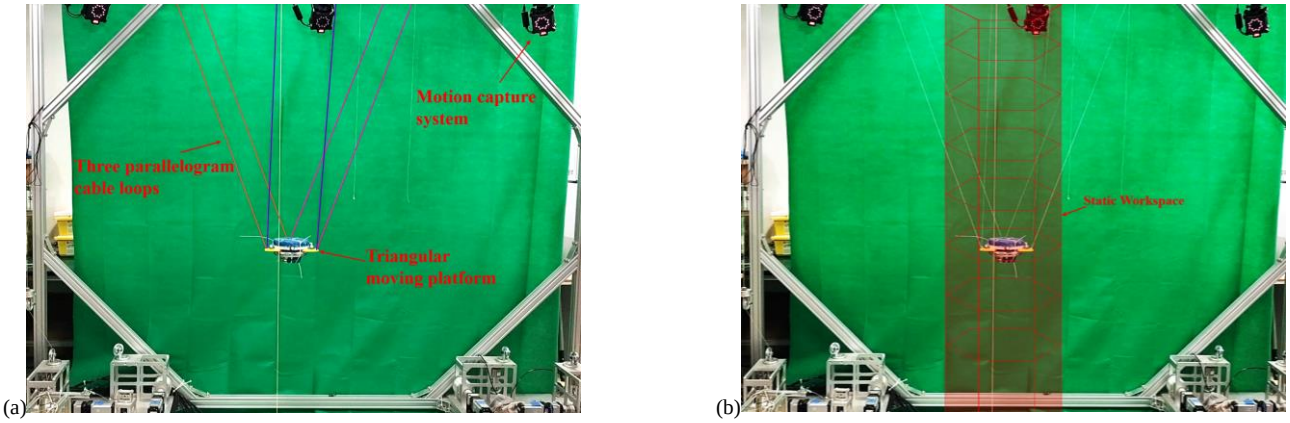

Fig. 4. (a) Experiment setup and (b) static workspace of the CSPR.

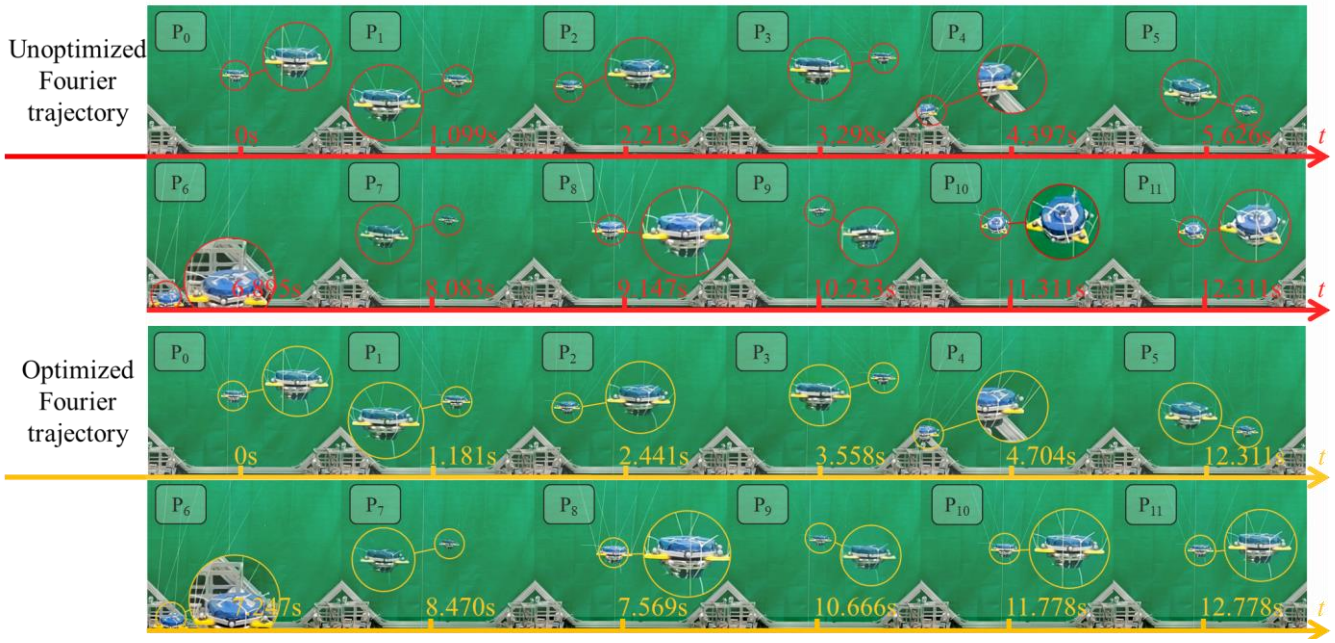

Fig. 5. Comparison of Fourier trajectories before and after optimization.

TABLE I
CONFIGURATION PARAMETERS

Exit points	Position	Attachment points	Position	Exit points	Position	Attachment points	Position	Exit points	Position	Attachment points	Position
A_{11}	[57.7,-100, 0]	B_{11}	[609.2,-100.0, 0]	A_{21}	[57.7, 100, 0]	B_{21}	[-218.0, 560.9, 0]	A_{31}	[-115.5, 0, 0]	B_{31}	[-391.2,-460.9, 0]
A_{12}	[57.7, 100, 0]	B_{12}	[609.2, 100.0, 0]	A_{22}	[-115.5, 0, 0]	B_{22}	[-391.2, 460.9, 0]	A_{32}	[57.7,-100, 0]	B_{32}	[-218.0,-560.9, 0]

TABLE II
TARGET POINT POSITIONS

Target points	Position	Target points	Position
P_0	[0, 0, 1200]	P_6	[700, -500, 1600]
P_1	[200, 250, 1200]	P_7	[-900, 300, 1200]
P_2	[- 50, -500, 1300]	P_8	[800, -100, 1100]
P_3	[-150, 700, 1000]	P_9	[-600, 100, 1150]
P_4	[430, -700, 1400]	P_{10}	[300, -50, 1150]
P_5	[-600, 600, 1600]	P_{11}	[0, 0, 1200]

TABLE III
THE FREQUENCY COEFFICIENTS AFTER OPTIMIZATION

Segments	$\omega_i/\omega_{i,g}$	Segments	$\omega_i/\omega_{i,g}$
P_0~ P_1	0.801	P_6~ P_7	0.957
P_1~ P_2	0.879	P_7~ P_8	0.947
P_2~ P_3	0.954	P_8~ P_9	0.981
P_3~ P_4	0.971	P_9~ P_{10}	1.015
P_4~ P_5	0.994	P_{10}~ P_{11}	0.801
P_5~ P_6	0.979		

B. The Fourier dynamic trajectory experiment

Target points are given in Table II. The velocity at target points is set to 0 while ensuring continuous acceleration. Both the Fourier dynamic trajectories before and after optimization are experimented, as depicted in Fig. 5. The constraint on the lowest frequency is selected as k=0.8, and the frequency coefficients after optimization are displayed in Table III. For the trajectory without optimization, the moving platform becomes unstable and completely overturned after the P_{10} point. The tilt angle shown in Fig. 6 confirm that the moving platform lost control during the movement of P_9~P_{10}. However, after optimization, the moving platform successfully reached all target points with limited tilt angle. The terminal pose of the CSPR in experiments were measured by the NOKOV motion capture system, which offers an accuracy of 0.1mm/0.5° and operates at a frequency of 60 Hz. For detailed illustration, please refer to the attached videos.

The tilt angles of Fourier trajectories before and after optimization are compared in Fig. 6. Before optimization, the maximum tile angle reaches 22.1°, occurring between P_{10}~P_{11}. After optimization, the maximum tile angle reduced to 8.23°, occurring between P_5~P_6.

The tilt angle of moving platform during the dynamic trajectory is mainly determined by two factors:

1) Tilt sensitivity and cable length errors. The cable length error is mapped to the tilt angle through the tilt sensitivity determined by kinematics. Cable length errors stem from various factors, including inaccuracies in cable elasticity, cable exit and attachment points, and pulley and drum kinematics. These factors render the cable length error time-varying and non-linear. The sensitivity of the tilt angle to the cable length error is defined in [35] as

$$\sigma_r = \max_{\|\delta \boldsymbol{l}\|=1} \|\delta \boldsymbol{\varphi}\| . \tag{25.}$$

where $\delta \boldsymbol{l}$ is the vector of variation in cable length and $\delta \boldsymbol{\varphi}$ is the vector of variation in rotation.

The tilt sensitivity of the CSPR in the plane of z = 1000mm is illustrated in Fig. 7, with target points are projected onto the plane. Generally, as the moving platform moves away from the workspace center, the tilt sensitivity increases, resulting in an amplified tilt angle of the moving platform with each unit cable length change.

2) Torque-resistance performance. The dynamic tilting results in the generation of additional torques, alongside the existing parasitic tilting torques in the general configuration, which test the torque-resistance ability of CSPR as indicated by the TRAI and TRCI defined in this letter.

Three indexes (the TRAI, TRCI, and sensitivity) are plotted separately with the tilt angle in Fig. 8. By comparing the relationship between three indexes and the tilt angle before and after optimization, it can be found that 1) the TRCI is directly correlated with the dynamic tilt angle. When its value exceeds 1, the moving platform could overturn and the CSPR lose control; 2) Smaller TRAI and TRCI values indicate better resistance to disturbances, resulting in a smaller dynamic tilt angle; 3) When the TRAI and TRCI are both small, the tilt angle is primarily influenced by the tilt sensitivity, which is mainly determined by kinematics and cable errors.

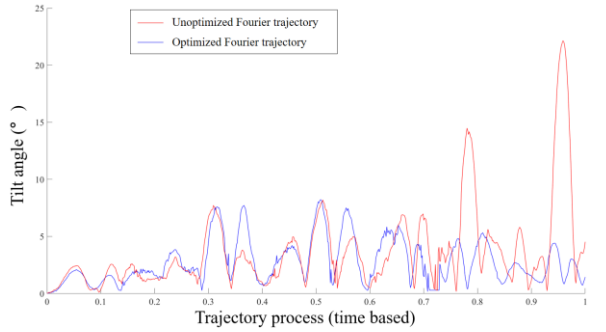

Fig. 6. Tilt angle values of Fourier trajectories before and after optimization.

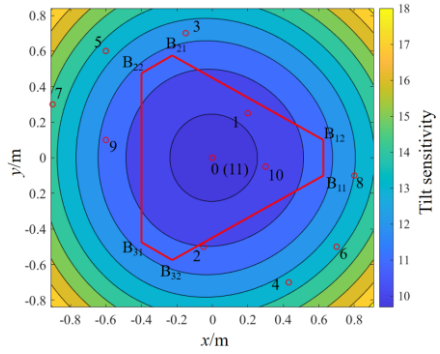

Fig. 7. Tilt sensitivity and point projections in the cross section of z = 1000mm.

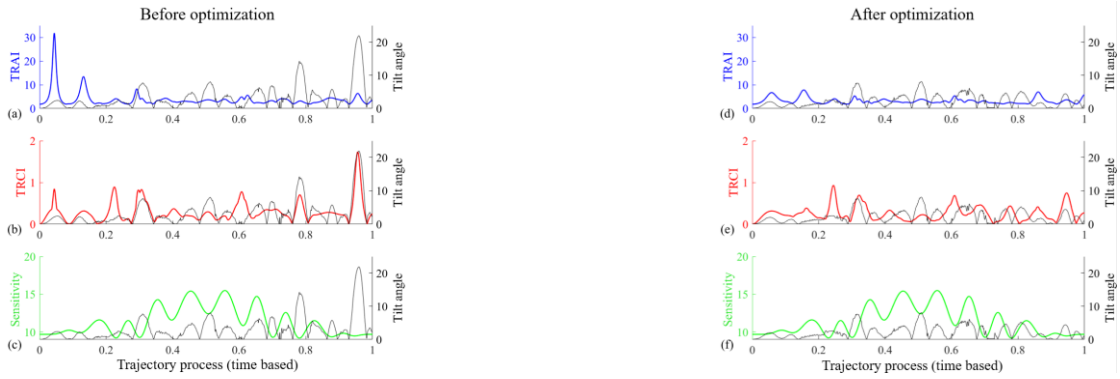

Fig. 8. Comparative display of the tilt angle (grey line) and the TRAI (blue line), TRCI (red line), sensitivity (green line) in (a), (b) and (c) before optimization, and in (d), (e) and (f) after optimization.

Results demonstrate that the optimization improves the torque resistance performance, the tile angle of moving platform is consistent with the tilt sensitivity, and the dynamic trajectory is applicable in the general configuration. Furthermore, the proposed indexes complement the tilt sensitivity, providing a comprehensive reflection and explanation of the tilt angle observed in the dynamic trajectory.

C. The B-spline dynamic trajectory experiment

In the B-spline dynamic trajectory experiment, target points with zero velocity constraints are consistent with Table II. The midpoints of trajectory are positioned 0.2m above the center of the line connecting two target points (except for the last two).

The fourth-order B-spline model is used to plan the three-point constrained dynamic trajectory in the experiment. The derived B-spline trajectory takes 12.311s, and 6.8% more efficient than the optimized Fourier trajectory, despite the longer route and additional midpoints. The dynamic trajectory and experiment results are illustrated in Fig. 9, and the experiment video is attached. The experimental results demonstrate that the CSPR successfully executed the proposed B-spline trajectory as expected. Minor position deviations occurred due to ignored cable elasticity, pulley kinematics and size errors of the reconfigurable experimental platform.

According to the data collected by the NOKOV system, the tilt angle of the moving platform during the dynamic trajectory does not exceed 7°. Velocity and acceleration of the moving platform are depicted in Fig. 10(a) and 10(b). Experimental and simulated results exhibit good agreement, with the desired velocity and acceleration precisely achieved.

The cable tensions of the B-spline dynamic trajectory are shown in Figs. 10(c). Cable tensions during the trajectory remain consistent with the simulated values. The frictions of multiple pulleys arranged between cable attachment points and tension sensors introduce some interference, while cable elasticity causes the actual cable tension to oscillate relative to the theoretical value.

V. Discuss and Conclusion

In this letter, we focus on the dynamic trajectory of general CSPRs with parallelogram cable loops for industry applications, such as palletizing and sorting. The decoupling of the force space and torque space is realized considering the properties of parallelogram cable loops. The available force set is separated from the available wrench set, which facilitates independent studies on the performance of CSPRs with translational DOFs. The torque-resistance ability indexes (the TRAI and TRCI) of the CSPR are defined to evaluate the ability of the moving platform to resist external torques.

A dynamic trajectory optimization method based on the proposed TRAI and TRCI indices is proposed. The Fourier model is applied to the dynamic trajectory planning of the CSPR with parallelogram cable loops, considering the general configurations. Experimental results reveal that despite having a smaller static workspace, the general CSPR can achieve a comparable dynamic motion range to that of CSPRs in special configurations. The trajectory optimization is implemented with the proposed indexes, which improve and eliminate the oscillation and overturn of the moving platform at the cost of a 7.3% increase in the runtime. Moreover, our experiments confirm that the optimization based on proposed torsion resistance indexes enhances resistance to parasitic-tilting, and proves dynamic trajectory with higher versatility to be used in general configuration. Furthermore, our experiments validate that the proposed indexes complement tilt sensitivity, providing a comprehensive indication of the tilt angle of the moving platform in dynamic trajectories.

By introducing B-splines, this letter realizes a flexible dynamic trajectory with obstacle avoidance ability. Simulation and experimental results showcase the higher flexibility and efficiency of proposed flexible dynamic trajectory. In the future, we will expand the scope of experimental validation, including the application and performance evaluation under different working conditions, driving performance improvements and practical applications of proposed dynamic trajectories.

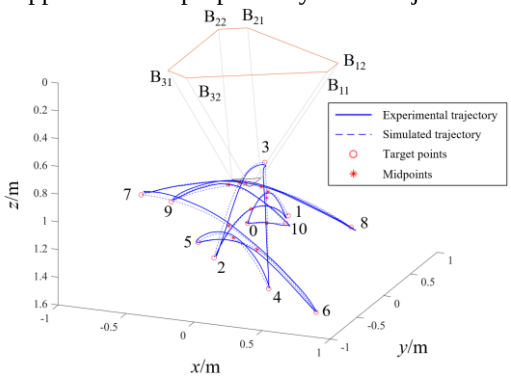

Fig. 9. Dynamic trajectory of the fourth-order B-spline model.

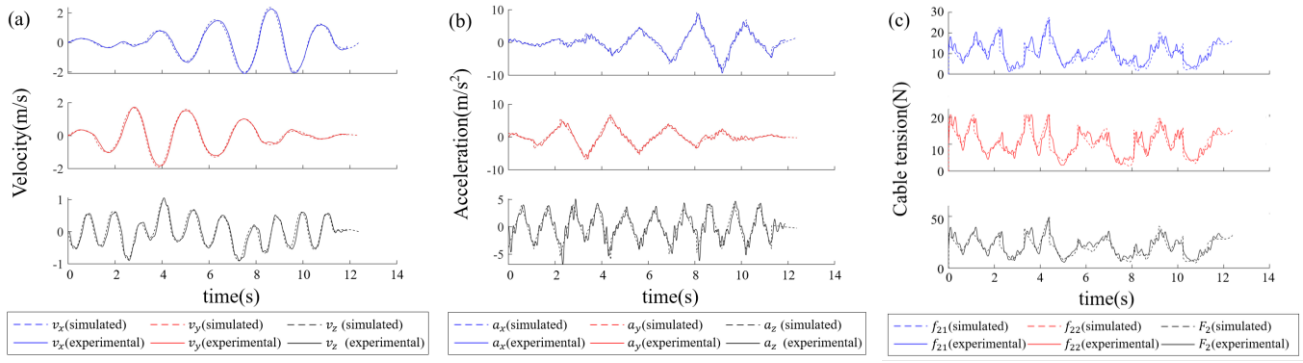

Fig. 10. Moving platform velocity (a), acceleration (b) and cable tensions (c) of the B-spline trajectory.

REFERENCES AND FOOTNOTES

[1] Z. Zhang, Z. Shao, and L. Wang, "Optimization and implementation of a high-speed 3-DOFs translational cable-driven parallel robot," *Mechanism and Machine Theory*, vol. 145, Mar. 2020.

[2] Z. Zhang, Z. Shao, and L. Wang, "Optimization and implementation of a high-speed 3-DOFs translational cable-driven parallel robot," *Mechanism and Machine Theory*, vol. 145, Mar. 2020.

[3] X. Tang, "An Overview of the Development for Cable-Driven Parallel Manipulator," *Advances in Mechanical Engineering*, vol. 6, Jan. 2014.

[4] B. Zi, B. Y. Duan, J. L. Du, and H. Bao, "Dynamic modeling and active control of a cable-suspended parallel robot," *Mechatronics*, vol. 18, no. 1, pp. 1-12, Feb. 2008.

[5] C. Gosselin, "Cable-driven parallel mechanisms: state of the art and perspectives," *Mechanical Engineering Reviews*, vol. 1, no. 1, pp. DSM0004-DSM0004, Jan. 2014.

[6] M. Tanaka, Y. Seguchi, S. Shimada, "Kineto-statics of skycam-type wire transport system," In *Proceedings of USA-Japan Symposium on Flexible Automation, Crossing Bridges: Advances in Flexible Automation and Robotics*, Minneapolis, Minnesota, USA, 1988, pp. 689-694.

[7] R. Bostelman, J. Albus, N. Dagalakis, A. Jacoff, and J. Gross, "Applications of the NIST RoboCrane," In *Proceedings of the 5th International Symposium on Robotics and Manufacturing*, Maui, HI: NIST, 1994.

[8] J. Duan, Z. Shao, Z. Zhang, and F. Peng, "Performance Simulation and Energetic Analysis of TBot High-Speed Cable-Driven Parallel Robot," *Journal of Mechanisms and Robotics*, vol. 14, no. 2, Apr. 2021.

[9] Z. Qin, Z. Liu, Y. Liu, H. Gao, C. Sun, and G. Sun, "Workspace analysis and optimal design of dual cable-suspended robots for construction," *Mechanism and Machine Theory*, vol. 171, May. 2022.

[10] P. Bosscher, R. L. Williams, L. S. Bryson, and D. Castro-Lacouture, "Cable-suspended robotic contour crafting system," *Automation in Construction*, vol. 17, no. 1, pp. 45-55, 2007, Pages 45-55, Nov.2007.

[11] S. Lessanibahri, P. Cardou, S. Caro, "Parasitic Inclinations in Cable-Driven Parallel Robots using Cable Loops," In *Procedia CIRP*, Nantes, France, 2018, pp. 296-301.

[12] L. Étienne, P. Cardou, M. Métillon, and S. Caro, (April 21, 2022). "Design of a Planar Cable-Driven Parallel Crane Without Parasitic Tilt," *ASME. J. Mechanisms Robotics*, vol. 14, no. 4 Aug. 2022.

[13] P. Bosscher, R. L. Williams, & M. Tummino, "A Concept for Rapidly-Deployable Cable Robot Search and Rescue Systems," In *International Design Engineering Technical Conferences and Computers and Information in Engineering Conference*, Long Beach, California, USA, 2005, pp. 589-598.

[14] E. Barnett, C. Gosselin, "Large-scale 3D printing with a cable-suspended robot," *Additive Manufacturing*, vol. 7, pp. 27-44, Jul. 2015.

[15] G. Castelli, E. Ottaviano, and P. Rea, "A Cartesian Cable-Suspended Robot for improving end-users' mobility in an urban environment," *Robotics and Computer-Integrated Manufacturing*, vol. 30, no. 3, pp. 335-343, Jun. 2014.

[16] C. Gosselin, R. Ping, and S. Foucault, "Dynamic trajectory planning of a two-DOF cable-suspended parallel robot," in *2012 IEEE International Conference on Robotics and Automation*, Saint Paul, MN, 2012, pp. 1476-1481.

[17] C. Gosselin and S. Foucault, "Dynamic Point-to-Point Trajectory Planning of a Two-DOF Cable-Suspended Parallel Robot," IEEE Transactions on Robotics, vol. 30, no. 3, pp. 728-736, Jun. 2014.

[18] G. Mottola, C. Gosselin, and M. Carricato, "Dynamically Feasible Periodic Trajectories for Generic Spatial Three-Degree-of-Freedom Cable-Suspended Parallel Robots," *Journal of Mechanisms and Robotics*, vol. 10, no. 3, Jun. 2018.

[19] X. Jiang and C. Gosselin, "Dynamic Point-to-Point Trajectory Planning of a Three-DOF Cable-Suspended Parallel Robot," IEEE Transactions on Robotics, vol. 32, no. 6, pp. 1550-1557, Dec. 2016.

[20] X. Jiang and C. Gosselin, "Dynamically Feasible Trajectories for Three-DOF Planar Cable-Suspended Parallel Robots," In *Proceedings of the ASME 2014 International Design Engineering Technical Conferences and Computers and Information in Engineering Conference*, New York, USA, 2014.

[21] X. Jiang, E. Barnett, and C. Gosselin, "Dynamic Point-to-Point Trajectory Planning Beyond the Static Workspace for Six-DOF Cable-Suspended Parallel Robots," *IEEE Transactions on Robotics*, vol. 34, no. 3, pp. 781-793, Jun. 2018.

[22] J. M. Longval and C. Gosselin, "Dynamic Trajectory Planning and Geometric Design of a Two-DOF Translational Cable-Suspended Planar Parallel Robot Using a Parallelogram Cable Loop," In Proceedings of the ASME 2018 International Design Engineering Technical Conferences and Computers and Information in Engineering Conference, Quebec City, Quebec, Canada, 2018.

[23] G. Mottola, C. Gosselin, and M. Carricato, "Dynamically feasible motions of a class of purely-translational cable-suspended parallel robots," *Mechanism and Machine Theory*, vol. 132, pp. 193-206, Feb. 2019.

[24] S. Qian, K. Bao, B. Zi, and W. D. Zhu, "Dynamic Trajectory Planning for a Three Degrees-of-Freedom Cable-Driven Parallel Robot Using Quintic B-Splines." *ASME. J. Mech. Des*, vol. 142, no.7, Jul. 2020.

[25] S. Bouchard, C. Gosselin, B. Moore, "On the ability of a cable-driven robot to generate a prescribed set of wrenches," *Journal of Mechanisms and Robotics-Transactions of the ASME*, vol.2, no. 1, Feb. 2010.

[26] T. Rasheed, P. Long, S. Caro, "Wrench-feasible workspace of mobile cable-driven parallel robots," *Journal of Mechanisms and Robotics-Transactions of the ASME*, vol.12, no.3, Jan. 2020.

[27] E. Jonathan, D. Lau, Y. Tan, and D. Oemtomo, "Available acceleration set for the study of motion capabilities for cable-driven robots," *Mechanism and Machine Theory*, vol. 105, pp. 320-336, Nov. 2016.

[28] J. Erskine, A. Chriette, S. Caro, "Wrench analysis of cable-suspended parallel robots actuated by quadrotor unmanned aerial vehicles," *Journal of Mechanisms and Robotics-Transactions of the ASME*, vol.11, no.2, Apr. 2019.

[29] S.B. Liu, J.P. Mei, P.F. Wang, and F. Guo, "Optimal design of a coupling-input cable-driven parallel robot with passive limbs based on force space analysis," *Mechanism and Machine Theory*, vol. 184, Jun. 2023.

[30] J. Erskine, A. Chriette, and S.Caro, "Wrench Capability Analysis of Aerial Cable Towed Systems." In *Proceedings of the ASME 2018 International Design Engineering Technical Conferences and Computers and Information in Engineering Conference*, Quebec City, Quebec, Canada, 2018.

[31] G. El-Ghazaly, M. Gouttefarde, V. Creuze and F. Pierrot, "Maximum wrench feasible payload in cable-driven parallel robots equipped with a serial robot," *In 2016 IEEE International Conference on Advanced Intelligent Mechatronics (AIM)*, Banff, AB, Canada, 2016, pp. 1572-1578.

[32] Y. Sun, Y. Guo, C. Song, and D. Lau, "Wrench-feasible workspace-based design of hybrid thruster and cable driven parallel robots," *Mechanism and Machine Theory*, vol. 172, Jun. 2022.

[33] C. B. Pham, S. H. Yeo, G. Yang, and I. M. Chen, "Workspace analysis of fully restrained cable-driven manipulators," *Robotics and Autonomous Systems*, vol. 57, no. 9, pp. 901-912, Sep. 2009.

[34] X. Tang, L. Tang, J. Wang, and D. Sun, "Workspace quality analysis and application for a completely restrained 3-Dof planar cable-driven parallel manipulator," *Journal of Mechanical Science and Technology*, vol. 27, no. 8, pp. 2391-2399, Aug. 2013.

[35] P. Cardou, S. Bouchard and C. Gosselin, "Kinematic-Sensitivity Indices for Dimensionally Nonhomogeneous Jacobian Matrices," *IEEE Transactions on Robotics*, vol. 26, no. 1, pp. 166-173, Feb. 2010.